Effective pathogens inactivation in air ducts through UVC light

M. Lombini[1], A. Bianco[2], F. Cortecchia[1], A. De Rosa[1], E. Diolaiti[1], M. Fiorini[4], L. Lessio[3], A. Macchi[2], G. Malaguti[1] G. Pareschi[2], D. Rovetta[5], L. Treccani[5] and G. Zanetti[5]

[1] Istituto Nazionale di Astrofisica - Osservatorio di Astrofisica e Scienza dello Spazio di Bologna, Via Gobetti 93/3, I-40129 Bologna, Italy
[2] Istituto Nazionale di Astrofisica - Osservatorio Astronomico di Brera, Via E. Bianchi 46, I-23807 Merate (Lc), Italy
[3] Istituto Nazionale di Astrofisica - Osservatorio Astronomico di Padova, Vicolo dell'Osservatorio 5, I-35122 Padova, Italy
[4] Istituto Nazionale di Astrofisica - Istituto di Astrofisica Spaziale e Fisica Cosmica di Milano, Via Alfonso Corti 12, I-20133 Milano, Italy
[5] Centro Servizi Multisettoriale e Tecnologico, Via Branze 45, I-25123 Brescia, Italy
e-mail: matteo.lombini@inaf.it

Abstract. The inactivation of airborne pathogens inside closed spaces is a critical issue, raised overwhelmingly during the current SARS-CoV 2 pandemic. Ultraviolet germicidal irradiation is a well-established technique that can effectively inactivate pathogens. In domestic and industrial air conditioning systems, large amounts of air flux can be sanified using mercury vapour lamps and proper shape and coating of a section of the air ducts. This paper describes the design of the UVC filter for air treatment unit which is in the installation phase at the headquarter of Centro Servizi Multisettoriale e Tecnologico in Brescia, Italy. The filter increased efficiency relies on concept of optical cavity, thanks to its shape and sources positions. Optical simulations have been carried out using a ray-tracing program, which has permitted to vary the parameters in order to maximise the internal irradiance quickly and thus the performance.

Key words. Radiation mechanisms: Ultraviolet general

1. Introduction

Microorganism transmission via air can elicit adverse human health effects, including infection, allergic reaction, inflammation, and respiratory diseases.

The coronavirus SARS-Cov 2 (Zhu et al. 2020) pandemic, started at the beginning of 2020, has drastically highlighted this aspect. Very soon, there was substantial evidence that airborne transmission was the virus most significant in-

fectious pathway (Cai et al. 2020; Jarvis 2020; Tang et al. 2020). Thus, our research has been focused on Ultraviolet Germicidal Irradiation (UVGI), a well-known technique for airborne pathogens inactivation (Kowalski 2010; Coohill & Sagripanti 2008) used for more than a century (Downes & Blunt 1877, 1879). The UVGI triggers the pathogen inactivation when the UVC photons, between 220 and 280 nm in wavelength, are absorbed by DNA/RNA(Beck et al. 2016).

Regarding the airborne pathogens, different reviews describe both the UVGI techniques (Reed 2010; Kowalski 2010) and the measurements of reference inactivation dosages (Lee 2011; Kim & Kang 2018).

Different pathogens require a different UVC irradiation dose for successful inactivation (Kowalski 2010; Malayeri et al. 2016) and the inactivation rate depends on the irradiation wavelength (Gerchman et al. 2020). The inactivation doses for aerosol applications also depend on relative humidity (RH) (McDevitt et al. 2012; Tseng & Li 2005), and on an effective filtration of dust (Eisenlöffel et al. 2019), which absorbs light and shields pathogens.

The most used source for UVGI applications is the mercury-vapour lamp. This source emits radiation with a peak at 253.7 nm when an electrical current in the gas excites mercury vapour atoms inside the quartz envelope (mainly cylindrical). In 2013, it was decided to forbid mercury-containing merchandise by 2020 for the protection of human and environmental health (Kessler 2013). Nevertheless, mercury UVC lamps are still used in UVGI systems because of their sufficiently high emission power and reasonable cost, compared to the still very expensive UVC LEDs.

This paper describes the design of a demonstrator of a filter for the sanification of air through UVC light for the Air Treatment Unit (ATU) plant of the Centro Servizi Multisettoriale e Tecnologico (CSMT) located in Brescia,

Italy. The filter has been being installed and it will be tested in the next months. The filter is intended to be a highly reflective cavity, replacing a portion of the recirculating air duct of the building, where the internal volume is illuminated with mercury vapour lamps light, which is bounded as much as possible by proper positioning of the sources and shape of the filter. For the optical design and efficiency calculations, we have used the ray-tracing software Zemax OpticStudio®, already used to estimate the performance of UVGI devices (Luo & Zhong 2021; Purschke et al. 2020; Wilde et al. 2020; Lau et al. 2012). The added value of using ray-tracing is the possibility of easily varying the system parameters and trying to maximise the inactivation performance.

2. UVGI fundamentals

The most appropriate unit of measure is the *fluence rate* (FR) since light travel directions are homogenised by multiple reflecting and scattering inside the filter (Ryan et al. 2010; Thatcher & Adams 2020). FR is defined as the radiant power passing from all directions through an infinitesimally small sphere of cross-sectional area δA, divided by δA, with typical units of mW/cm^2. *Fluence* (F), also called UV dose, is the total radiant energy from all directions passing through an infinitesimally small sphere of cross-sectional area δA, divided by δA, with typical units of mJ/cm^2.

The inactivation of the pathogens is a function of the total UV energy absorbed. A simplified model (Kowalski 2010) is the exponential relationship:

$$S = \frac{N}{N_0} = e^{-ktFR} = e^{-kF} \qquad (1)$$

where S is the survival fraction of microorganisms after being exposed to UVC light, N_0 is the number of survived microorganisms before the UVC exposure, N is the number of microorganisms after the UVC exposure, k is the specific rate constant unique to each type of microorgan-

ism (cm^2/mJ), FR is the fluence rate, t is the time interval, and $F = t \times FR$ is the fluence (mJ/cm^2). For high enough fluence values, the product high-intensity fluence rate short-time irradiation has the same sterilisation effect as the low-intensity fluence rate long-time irradiation (Sun et al. 2019).

3. Filter design
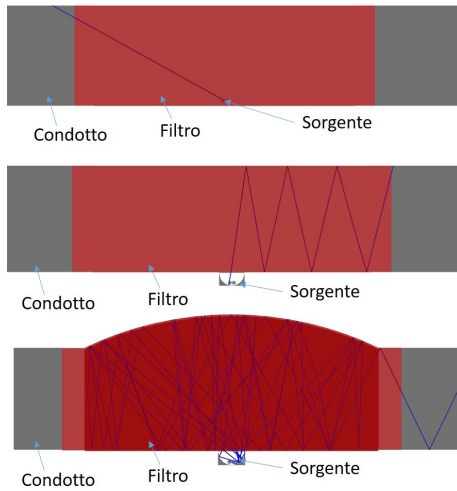
Fig. 1. Trade-off of the filter geometry and source position. The source is a cylinder with the axis perpendicular to the duct. Configuration 1 (top image) has the source inside the duct. Some light exits the filter without being reflected by the high reflective surfaces. Central image shows Configuration 2, where the source is outside the duct section and light is statistically reflected a few times before exiting the filter volume. Bottom image shows the rounded filter case (Configuration 3), where rays are subjected to be reflected toward the filter center.

The UVC filter under investigation has to replace a portion of the ATU duct, having a sectional size of 500 mm x 450 mm for a maximum length of 1500 mm, at CSMT headquarter. Some space around the duct is available and has been occupied since the chosen filter design has a rounded profile as shown in figure 2. The already mentioned optical cavity concept used to increase the fluence rate inside the filter has been described first by Jensen (1964) and similar experiments can be found in more recent works (Ryan et al. 2010; Zhang et al. 2020; Thatcher & Adams 2020). The magnification or enhancing factor for a closed cavity can be calculated from the material reflectivity R and has an exponential power law (Lombini et al. 2021b).

In reality, some light leaks the cavity or is absorbed by the external duct or hit the protective glass windows. Thus the enhancing factor is reduced compared to the theoretical one, but still, the reflectivity of the internal surfaces is a fundamental parameter for the filter efficiency. Since no secondary effects are produced after light absorption by pathogens (or air), the total UVC light total dose can be administered 'in pieces' after any of the numerous internal reflections, according to the Bunsen and Roscoe law (Schindl et al. 2001).

The internal surfaces of the filter are coated with Alanod MIRO UV C (ALANOD GmbH & Co. KG 2020), an aluminium foil coated with UVC highly reflective material (about 93% at 253nm), which can be delivered in large sheets and cut and bended for the project needs. The scattering data of Alanod at the working wavelength is unknown to the authors. When simulating it, we considered the data set provided by the supplier, measured at a longer wavelength, where the FWHM of the scattered rays cone angle around the specular reflection direction is about 5°. The duct outside the filter is supposed to be composed of a UVC absorbing material. The protecting windows which separate the source from the duct in the central and bottom images of Figure 1 are made of UV-graded silica, with a transmissivity > 90% at 254 nm.

4. Optical simulations

A typical issue when dealing with multiple reflections is the number of child rays generated from the parent one. The ray-tracing calculations continue until the ray's power has fallen below a defined fraction of the initial value or when the maximum allowed number of segments from the parent ray is reached. For $R = 0.99$ and a threshold of $1e - 6$ regarding the minimum relative ray intensity compared to the initial ray, the maximum number of reflection is ≈ 1400. Also, regarding the refraction and scattering, the issue is the exponential increase, at every interface, of the number of segments, considering creating only two segments after any interface. To avoid terminating calculations with the ray's power still above the threshold, only one new ray is generated after a reflection from a scattering or refractive surface. The number of segments adopted in the simulations is 2500, so far enough. Adequate sampling of the fluence rate inside the filter due to the scattering distribution has been guaranteed by a sufficiently high number of starting rays from each source, clearly at the price of a higher computational time.

The performance of the optical simulations in Zemax has been evaluated through 'detectors', which are plane or volume arrays that record the power of all the rays passing through the surface or volume. A plane array was placed at the end of one of the two flanges with its surface perpendicular to the filter axis to measure the amount of radiation exiting the cavity. The fluence rate inside the cavity (and the flanges) has been evaluated by a volumetric detector, a three-dimensional array formed by cubic voxels, each one of $10mm^3$ to sample the fluence rate's spatial variations adequately. The way to pass from the volumetric power density P_V, whose unit of measure is W/m^3 (or mW/cm^3), To the Fluence rate, whose unit of measure is W/m^2 (or mW/cm^2), is to transform the volumetric power density values from the optical simulations to surface power density FR_A from rays entering the cube through each of the six surfaces with area A.

4.1. Geometry trade-off

We describe three possible filter configurations with different shapes and source positions. These simulations aimed to find out the efficiency gain versus the constructive complexity. Figure 1 shows the three configurations. The top image shows configuration 1, a filter with the same section of the outer duct and a cylindrical source inside the filter volume. The central image, configuration 2, differs for the position of the source, which has been inserted inside a parabolic toroidal reflector outside the duct footprint. The reflector has the same reflectivity as the filter, and some investigations have been performed to retrieve the optimal size, curvature and source position. A UV grade window seals the parabolic reflector volume for safety reasons, in case the lamp would break and pollute the air with mercury vapours. The bottom image shows configuration 3, a filter with curved surfaces on three sides and the source inside the parabolic reflector as for the previous case. Figure 2 illustrates that the performance comparison has been made on the fluence rate inside the filter. Configuration 1, where the source is inside the volume, has a reduced performance compared to the other two configurations because some light exiting the source goes directly outside the filter. Thus the multiple reflections do not occur for those rays. In configuration 2, the rays leaving the source cannot reach the filter directly, and one or more reflections occur. Moreover, optimising the reflector parameters has permitted the maximisation of the filter efficiency. Configuration 3 behaves much more as an optical cavity due to both the external position of the source and the curved profile of the filter. Rays are reflected toward the inside of the filter, and thus the mean number of reflections from the highly reflective internal surfaces is increased. Configuration 3 of the filter has higher efficiency with an exter-

nal source and curved profile. It has been decided to perform fluid-dynamic simulations and design an actual device within the same features. The calculations on the estimated efficiency give that configurations 2 and 3 show, respectively, an increase in the FR inside the filter of 1.5 and 2.5 compared to configuration 1. For this reason, it has been decided to build the filter with three rounded sides, and this filter geometry has been patented (Lombini et al. 2021a).

5. Filter design
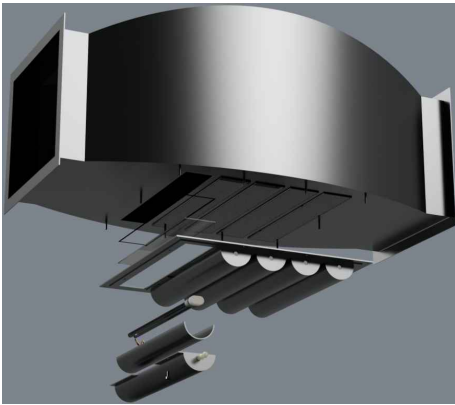
Fig. 2. Exploded 3d image of the filter to be installed at CSMT ATU duct.

The exploded mechanical design of the filter to be installed at the CSMT ATU duct is shown in Figure 2. The filter envelope has a rounded profile on three sides (curvature radius of 1500 mm) and has the internal surfaces made of Alanod. Five sources, each with a power of 17 W, are placed on the parabolic reflectors along the filter plane side. The reflector volumes are sealed with UV graded glasses (2 mm thick and 90% transmissivity) for safety reasons to avoid pollution inside the duct if the mercury lamp breaks. The filter parameters have been optimised considering both the efficiency and components availability.

5.1. Air flow

The Computational Fluid Dynamic (CFD) analysis has been performed using the Ansys CFX5 software. The voxels are all hex elements with dimensions of 10 mm, and the material is air at 25° C. The ATU maximum flow is 5000 m^3/h, corresponding to a boundary condition at the filter inlet of 6.17 m/s. A turbulence fraction of 5% has been considered, while the outlet is an opening at the normal ambient pressure. Simulations results gave a laminar flow inside the filter. Thus the air trajectories can be considered independent. Figure 3 shows the velocity field along the two planes along the longitudinal cross-sect inside the filter. The velocity slows down inside the cavity, where the sectional area is larger. Due to the high flow, most air tends to remain in almost straight trajectories, and a noticeable reduction appears when increasing the distance from the optical axis. Closer to the cavity walls, some air re-circulation is present. Re-circulation zones are not considered in the filter efficiency calculations, described in Section 5.2.

5.2. Expected efficiency

We have combined the fluence rate results with airflow flow simulations to obtain the fluence and consequently the survival fractions SF.

Given the filter parameters and the microorganism rate constant k:

- the velocity field from CFD simulations is transformed to a residence time field and multiplied by the FR spatial distribution to obtain the locally delivered F in each cell;
- the airflow is discretized in n axial paths following the particle trajectories. The paths sections have a fractional area a_n of the entering area A;
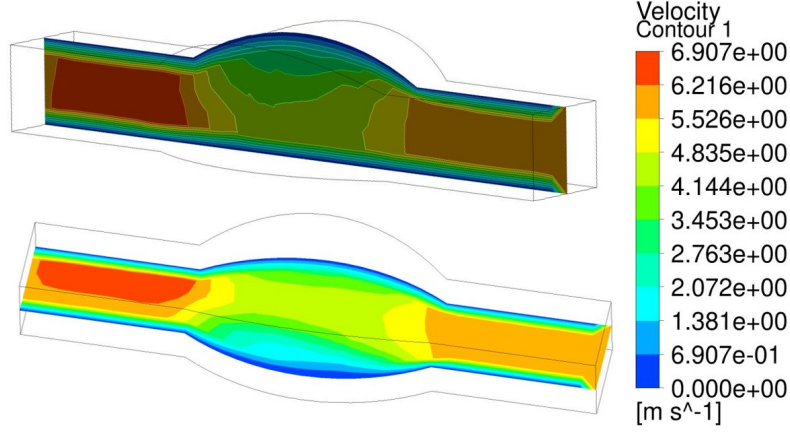
Fig. 3. a) Longitudinal and transverse sections of the filter where the air velocity field is displayed. Entrance air, the flow is from right to left in the images, has a velocity of v_{in} is 6.2 m/s. The no uniformity on the exit side of the transverse section is the output of a single simulation outcome, to be averaged with other realizations.

– each path is divided into z cells and the survival fraction SF_n is calculated:

$$SF_n = \prod_z SF_{n,z} = (e^{-k\sum t_{n,z}FR_{n,z}}) \cdot a_n \tag{2}$$

– the overall survival fraction SF is the sum of the survival fractions of each path

$$SF = \sum_n SF_n \tag{3}$$

– we can define the equivalent fluence F_{eq} as the fluence that delivers the same survival fraction SF_v as the filter with the calculations from above steps.

$$SF_v = e^{-kF_{eq}} \rightarrow F_{eq} = -\frac{log(SF_v)}{k} \tag{4}$$

For the simulated case, $F_{eq} > 14 mJ/cm^2$

Regarding the case of SARS-Cov 2, different reviews agree that about 3-4 mJ/cm^2 are sufficient to produce at least a log2 inactivation rate (99%) (Biasin et al. 2021; Kowalski et al. 2020; Inagaki et al. 2020) Although the studies on the minimum infectious dose of SARS-Cov 2 for humans are not conclusive (Karimzadeh et al. 2021), it is clear that the littler the survival fraction, the better.

The filter efficiency is expected to be evaluated by means of measurement regarding the internal spatial FR. Since light is expected to be almost omnidirectional and UVC radiometers can measure light arriving over a certain solid angle, if the cosine correction to the recorded data is applied, a possible measurement could be performed utilising chemical actinometry (Koller 1965; Rahn 2004; Rahn et al. 2006). The SF performance can be measured by using a similar set-up as other experiments (Myatt et al. 2003; Peccia et al. 2001; Qiao et al. 2021; Thatcher & Adams 2020; Ryan et al. 2010; Walker & Ko 2007).

The monitoring of Relative Humidity, temperature and dust will be activated after the testing phase. The effects of these parameters variation on the inactivation

rate efficiency are not foreseen to be evaluated for the pilot plant.

6. Conclusions

We have described the design of the UVC filter for the ATU in the CSMT headquarter, highlighting the technical motivation of the chosen design and presenting the estimated performance. After the installation, tests regarding the internal fluence rate and the inactivation efficiency will be performed. Final test are expected to be carried out by Spring 2022. We are confident that the system will be very effective at inactivating SARS-CoV 2, even for the maximum air flux as described in Section 5.2.

Ray-racing and CFD analyses have been fundamental to producing a realistic and accurate performance estimation since analytical formulas to estimate source emission power and spatial irradiation could not be precise enough. The light is emitted in the filter's internal volume, reflected and scattered in all directions. The fluence rate calculations have been carried out by considering volumetric units and successively transformed into surface units to be consistent with the standard units of measures.

The described filter is a pilot device which has the aim to demonstrate the inactivation efficacy of the UVC exposure in a reflecting cavity. Further improvements regarding the reflectivity increase or a different filter shape are foreseen in the next future.

References

ALANOD GmbH & Co. KG. 2020, *UV Light Applications*, SNAS548D, 2020. [Online]

Beck, S. E., Rodriguez, R. A., Hawkins, M. A., et al. 2016, Applied and environmental microbiology, 82, 1468

Biasin, M., Bianco, A., Pareschi, G., et al. 2021, Scientific Reports, 11, 1

Cai, J., Sun, W., Huang, J., et al. 2020, Emerging infectious diseases, 26, 1343

Coohill, T. P. & Sagripanti, J.-L. 2008, Photochemistry and photobiology, 84, 1084

Downes, A. & Blunt, T. P. 1877, Nature, 16, 218

Downes, A. & Blunt, T. P. 1879, Proceedings of the Royal Society of London, 28, 199

Eisenlöffel, L., Reutter, T., Horn, M., et al. 2019, PLOS ONE, 14, 1

Gerchman, Y., Mamane, H., Friedman, N., & Mandelboim, M. 2020, Journal of Photochemistry and Photobiology B: Biology, 212, 112044

Inagaki, H., Saito, A., Sugiyama, H., Okabayashi, T., & Fujimoto, S. 2020, Emerging Microbes & Infections, 9, 1744

Jarvis, M. C. 2020, Frontiers in Public Health, 8, 813

Jensen, M. M. 1964, Applied and Environmental Microbiology, 12, 418

Karimzadeh, S., Bhopal, R., & Tien, H. N. 2021, Epidemiology & Infection, 149

Kessler, R. 2013, The Minamata Convention on Mercury: a first step toward protecting future generations

Kim, D.-K. & Kang, D.-H. 2018, Applied and environmental microbiology, 84

Koller, L. R. 1965, Ultraviolet radiation (John Wiley and Sons)

Kowalski, W. 2010, Ultraviolet germicidal irradiation handbook: UVGI for air and surface disinfection (Springer science and business media)

Kowalski, W., Walsh, T., & Petraitis, V. 2020, Purplesun Inc

Lau, J., Bahnfleth, W., Mistrick, R., & Kompare, D. 2012, HVAC&R Research, 18, 626

Lee, B. U. 2011, Aerosol and Air Quality Research, 11, 921

Lombini, M., Bianco, A., Cortecchia, F., et al. 2021a, Patent title: device for the disinfection of a fluid flow in a duct using UV-C radiation

Lombini, M., Diolaiti, E., De Rosa, A., et al. 2021b, Optics Express, 29, 18688

Luo, H. & Zhong, L. 2021, Building and environment, 107852

Malayeri, A. H., Mohseni, M., Cairns, B., et al. 2016, IUVA News, 18, 4

McDevitt, J. J., Rudnick, S. N., & Radonovich, L. J. 2012, Applied and Environmental Microbiology, 78, 1666

Myatt, T. A., Johnston, S. L., Rudnick, S., & Milton, D. K. 2003, BMC Public Health, 3, 1

Peccia, J., Werth, H. M., Miller, S., & Hernandez, M. 2001, Aerosol Science and Technology, 35, 728

Purschke, M., Elsamaloty, M., Wilde, J. P., et al. 2020, Appl. Opt., 59, 7585

Qiao, Y., Yang, M., Marabella, I. A., et al. 2021, Environmental Science & Technology, 55, 4174, pMID: 33263988

Rahn, R. O. 2004, Photochemistry and photobiology, 80, 346

Rahn, R. O., Bolton, J., & Stefan, M. I. 2006, Photochemistry and Photobiology, 82, 611

Reed, N. G. 2010, Public health reports, 125, 15

Ryan, K., McCabe, K., Clements, N., Hernandez, M., & Miller, S. L. 2010, Aerosol Science and Technology, 44, 541

Schindl, A., Rosado-Schlosser, B., & Trautinger, F. 2001, Der Hautarzt; Zeitschrift fur Dermatologie, Venerologie, und verwandte Gebiete, 52, 779

Sun, T., Huang, C., Lui, P., Chen, Y., & Shieh, H. 2019, in 2019 IEEE Eurasia Conference on Biomedical Engineering, Healthcare and Sustainability (ECBIOS), 57–60

Tang, S., Mao, Y., Jones, R. M., et al. 2020, Environment international, 144, 106039

Thatcher, C. H. & Adams, B. R. 2020, Chemical Engineering Science, 230, 116204

Tseng, C.-C. & Li, C.-S. 2005, Aerosol Science and Technology, 39, 1136

Walker, C. M. & Ko, G. 2007, Environmental Science & Technology, 41, 5460

Wilde, J. P., Baer, T. M., & Hesselink, L. 2020, Applied Optics, 59, 7596

Zhang, H., Jin, X., Nunayon, S. S., & Lai, A. C. K. 2020, Indoor Air, 30, 500

Zhu, N., Zhang, D., Wang, W., et al. 2020, New England Journal of Medicine, 382, 727, pMID: 31978945